# A Mathematical Model for Dorsal Closure

Luis Almeida, Patrizia Bagnerini, Abderrahmane Habbal, Stéphane Noselli, Fanny Serman

# A Mathematical Model for Dorsal Closure

Luís Almeida[1], Patrizia Bagnerini[2], Abderrahmane Habbal[1], Stéphane Noselli[3] and Fanny Serman[1,3]

[1] *Laboratoire J.A. Dieudonné*
*Université de Nice*
*UMR 6621 CNRS*
*Parc Valrose*
*F-06108 NICE Cédex 02, FRANCE*

[2] *DIPTEM*
*Università degli Studi di Genova*
*P.le Kennedy-Pad D*
*16129 Genova, ITALY*

[3] *Institute of Developmental Biology & Cancer IBDC-Nice*
*Université de Nice*
*UMR 6543 CNRS*
*Parc Valrose*
*F-06108 NICE Cédex 02, FRANCE*

**Abstract**

During embryogenesis, Drosophila embryos undergo epithelial folding and unfolding, which leads to a hole in the dorsal epidermis, transiently covered by an extraembryonic tissue called the amnioserosa. Dorsal Closure (DC) consists of the migration of lateral epidermis towards the midline, covering the amnioserosa. We present here a simple mathematical model for DC that involves a reduced number of parameters directly linked to the intensity of the forces involved and which is applicable to a wide range of geometries of the Leading Edge. We validate this approach in a Wild Type setting and also test it further by obtaining variations of the force coefficients that are consistent with what was previously described for embryos where the zipping force is perturbed through the expression of Spastin (a microtubule severing protein).

*Preprint submitted to Journal of Theoretical Biology* *January 15, 2010*

*Keywords:*

This project was supported by the ACI NIM Momatsouti. Work in the SN laboratory is supported by CNRS, ANR, ARC, FRM, CEFIPRA.

## 1. Introduction

In this work we present a mathematical model of Dorsal Closure (DC) which is a widely used model for development and wound healing. DC consists of the convergence of lateral epidermal cells towards the midline covering the amnioserosa in a couple of hours (see figure 1 and movie `DC.mov`). As it progresses, the left and right margins of the Leading Edge (LE) are progressively knitted to each other in a zipping process and eventualy seal the hole leaving no traces of its prior existence. In spite of the fact that the lateral epidermis has to encompass an increasing amount of area, DC does not involve any cell division but only a coordinated reorganization and contraction of the actomyosin cytoskeleton in different populations of epithelial cells.

The cells in the dorsal-most row of the lateral epidermis are called the leading edge cells - these cells form the boundary of the lateral epidermis and they accumulate filamentous actin and myosin II (a motor protein) at their dorsal-most edge to form a contractile actomyosin cable. Such intercellular cable elements are anchored into adherens junctions between neighboring cells (which are locally reinforced for this purpose) and are thus all connected forming a supra-cellular acto-myosin cable that encircles the area covered by the Amniosersa. This cable structure is continuously put under tension by the myosin molecular motors making the actin filaments slide relative to each other thus producing a global contraction effect that helps closing the epithelial hole (since this is a dynamic process, new tension can be created by the molecular motors and the local cable tension does not necessarily decrease as the contraction proceeds). The position of this cable, at the boundary between the wound and the epidermis defines the Leading Edge (LE).

The hole is roughly shaped like an ellipse with major axis along the dorsal midline of the organism - which is along the anterior-posterior (AP) axis of the embryo. By convention, we will always display our images with the anterior on the left, the posterior on the right and a horizontal AP axis. The anterior and posterior ends of the hole are called the canthi - the LE has a rather singular geometry at these points. As indicated in figure 1, the

canthi separate the LE (also denoted $\omega_i$) into two halves - the top margin, denoted $\omega_i^t$, and the bottom margin, $\omega_i^b$ (in fact, in the original geometry of the embryo, these correspond to the right and left margins, respectively).

In (Kiehart et al. (2000)) DC was described as involving the following forces: 1) resistive tension from the stretched epidermis, 2) actin cable tension 3) amnioserosa contraction and 4) zipping.

The zipping force comes from the fact that LE cells extend actin protrusions, filopodia, that intertwine near the canthi drawing towards each other and knitting the two margins - the canthi advance towards the middle of the opening a bit like zippers (see movie `ZIP.mov`). The zipping process is essential for the proper matching of cells along the anterior-posterior axis. As the two margins merge during dorsal closure the cells from each side of the epidermis that meet end up establishing permanent (adherens) junctions similar to those between the other epidermal cells. At the same time the actin corresponding to the cable segment they contained is de-polymerised and in the end there is no trace remaining of the fact that they were far apart at the outset of DC.

In this paper we propose a simple model for simulating DC. Our approach is a natural generalization of the one proposed in Hutson et al. (2003) which consists of a system of two Ordinary Differential Equations (ODE) obtained by considering the balance of the forces described above in a very symetric setting where the LE is supposed to consist of the union of two arcs of circle. In that case it is sufficient to have one equation concerning the forces acting on the midpoint of each of these arcs plus a second equation to take the zipping into account. Here, we use a Partial Differential Equation (PDE) approach that allows us to go beyond these strong symetry assumptions (which had already been slightly relaxed in an ODE setting in Peralta et al. (2007)). A priori, the PDE setting allows us to consider quite general geometries and inhomogeneous forces. In practice, this generality implies optimizing a very big number of parameters which would be computationaly too costly and meaningless considering the precision of our data. Thus, we will present the case where the forces are supposed to be determined by a small number of coefficients and by the geometry of the LE (which can be quite general), as described below. We have already applied this type of model to Drosophila embryo wound healing in Almeida et al. (2009) obtaining quite satisfactory results (which confirms that this approach can deal with a wide range of hole geometries).

Each of the coefficients in our model is associated with one of the forces

described and will thus give us a way of measuring the relative contribution of that force (they are our force parameters). In fact, we make a movie of each embryo going through DC and extract the contours corresponding to the position of the LE at different times. For each movie, we then take the initial contour and, for a given set of force parameters, our PDE model can be used to simulate how this contour should evolve according to the model. We will optimize the set of force parameters so that the simulated contours fit the best way possible (i.e. in the way the minimizes an appropriate cost function defined below) the real contours extracted from the film up to the time DC is complete. This yields the force parameters of the embryo considered and is thus a way of measuring the relative intensities of these forces.

The way that these force coefficients change between wild type and mutant settings may give us a way of identifying which genes play an important role in regulating each of the forces present. Thus, we started by studying wild type (WT) embryos (n=10) and checked that the set of parameters obtained for the different embryos was consistent. This is a strong indication of the pertinence of the model in this setting.

We further challenged our model to see what it yielded in a setting where the microtubule severing protein Spastin was ubiquitously expressed in the tissues using the Armadillo-gal4 driver. Expression of this protein in engrailed half-segments of the lateral epidermis had been extensively studied in Jankovics and Brunner (2006) and they had observed that the zipping was significantly downregulated in this setting. In fact, as described in Jacinto et al. (2000), zipping requires the filopodia (and lamellipodia) whose formation depends on the actin organizing machinery which, as shown in Jankovics and Brunner (2006) is linked to microtubule activity. Our study of Arm-gal4-UAS-Spastin flies (n=10) shows that coefficient associated to zipping ($C_4$ in our model) we measured is considerably lower than that obtained in the WT setting. This is consistent with the results of Jankovics and Brunner (2006) and conforts us in the choice of this model.

Another advantage of our model is the direct way it links the coefficients we measure with the intensity of the associated forces. For instance in the case of the decrease of the zipping coefficient in the Spastin setting that we measure, this means that the zipping force in the model is lower (since $C_4$ is the intensity of that force term) whereas a decrease in the zipping rate $k_z$ (as defined in Hutson et al. (2003)) just directly means that the shape is changing in a different way (and it is this that is then associated with a difference in zipping).

## 2. Simple Mathematical Model

For mathematical purposes, the LE will also be denoted by $\omega$. Our simulation domain will be a rectangle, $M$, which contains the amnioserosa in the middle and part of the surrounding lateral epidermis all around it. The part of the domain occupied by the epidermis is $D = M \setminus W$ (see figure 1). The amnioserosa $W$ (and therefore also $D$) change in time. Actual mechanical behavior of the wound should at least obey nonlinear visco-elastic dynamics, involving a chemo-bio-mechanical coupling, as introduced in Olsen et al. (1995), Olsen et al. (1998) and Murray (2003). However, since epidermal wound closure occurs during a long time compared to the space scales involved, one may neglect inertial forces and consider the overall process as a succession of linear elastic equilibria, where we omit as well the successive initial stress fields. We will adopt such a so-called quasi-static approach to describe this evolution.

At each step $i = 1, \ldots, n$, $W_i$ and $D_i$ denote the positions of the amnioserosa and the ectoderm, and $\omega_i = \omega_i^t \cup \omega_i^b$ that of the LE (see figure 1). We suppose the behavior of the epidermis to be linearly elastic, homogeneous, isotropic and subject to four forces:

**1)** epidermal tension (that pulls the leading edges appart opposing the closure) which we simulate by constant normal forces applied at the top ($M^t$) and bottom ($M^b$) boundaries of our simulation domain. The actual forces should be considerably more complicated and are due to the stress fields induced by the previous morphogenetic movements (as well as those occurring during DC).

**2)** the actin cable tension. This term gives rise to a force that is proportional to the curvature at each point, in the spirit of what was described in Hutson et al. (2003) for the middle point of their arc of circle. Here, we extend this force to all the points on the LE - we work in a PDE framework instead of the ODE framework used in Hutson et al. (2003). It points towards the exterior of $D_i$ (i.e. towards the interior of the amnioserosa $W_i$) at the points of positive curvature of the LE and towards the its interior at points of negative curvature.

**3)** a uniform normal force pointing towards the exterior of $D_i$ - this force is associated to amnioserosa contraction (or lamellipodal crawling in a wound healing context - see Almeida et al. (2009)).

**4)** zipping at the canthi.

We will discuss a bit further this last term, i.e. the modeling of zipping, which plays a very important role in DC and which as mentioned above (based on Jankovics and Brunner (2006)) is the term that we expect to change significantly between the two settings we will consider in the present work (wild-type and Spastin). In general, we can model the zipping force ($Z$) by a term of the type

$$Z(x) = \int_{\omega} f(x,y)\frac{y-x}{|y-x|}dy \quad \text{for all } x \in \omega \ , \tag{1}$$

where $\omega$ is the Leading Edge (LE). Unfortunately, our present experimental tools and data do not enable us to obtain enough information about the function $f$ for precise modeling of its contribution. Nevertheless, we can assume that $f$ depends on the distance between the points ($|x-y|$). Indeed, we can write, $f(x,y) = g(|x-y|)h(x,y)$, where the function $g : \mathbb{R}^+ \to \mathbb{R}$ has compact support inside $|x-y| < 2L$, where $L$ is the maximum length of filopodia in the situation considered (it should depend on the particular fly line used).

As mentioned in Almeida et al. (2009), this approach should also be appropriate for modeling the zipping in wound healing as long as the wound $W$ (the set enclosed by the LE) is convex. In a general setting some caution should be needed in defining which filopodia can interact.

In DC, not only we are often in a convex setting, but we also have a particular geometry and behavior that simplifies the modeling of the zipping force. In the wild type setting (and most genetically modified settings we observed) there seems to be no zipping between points in the same margin, which implies that $f(x,y) = 0$ if $x$ and $y$ belong to the same margin (so, in practice, the integration in (1) is only over the opposite margin).

Moreover, the epidermis of the embryo is divided into 14 segments separated by sharp boundaries, each of them constituted by anterior and posterior cells (green and red cells, respectively, in movie `DC.mov`). This spatial organization is conserved at the end of DC by a proper segment adjustment potentially mediated by filopodia (Millard and Martin (2008)). Tracking of segment and parasegment boundaries during DC indicates that physical points on the leading edge move vertically, i.e. orthogonally to the AP axis (figure 2).

If we want to take into account the fact that zipping plays a role in segment matching then $f$ should also include specific information about the matching genes expressed by the cells present at points $x$ and $y$. In the wild type context, in the beginning of DC the parasegments that should match are placed (considering our orientation convention of horizontal AP axis and symmetry relative to this axis) vertically to their counterparts in the opposite leading edge. Moreover, according to figure 2, they move approximatively vertically throughout DC. In this work, we will consider only cases where we have this symmetry, and simulate them by supposing that we have a vertical zipping force which is supported in the part of the leading edge where the vertical distance between the two margins is smaller than $2L$. To be precise, for each step $i$, we suppose that the upper leading edge (denoted $\omega_i^t$) is described by a function $y = g_i(x)$ and the lower leading edge (denoted $\omega_i^b$) by $y = h_i(x)$ for $x \in [c_a, c_p]$ where $c_a$ and $c_p$ are the $x$ coordinates (horizontal positions) of the anterior and posterior canthi at step $i$. The zipping will then be effective only in the set $Z_i := \{(x, y) \in \omega_i \ : \ g_i(x) - h_i(x) \leq 2L\}$. We will consider more complex situations in the future.

Coming back to the global model of DC, the cytoskeleton and membrane of the cells of the epidermis are globally viewed as a mechanical continuum, which can bear traction and compression loads but not bending nor torsion. Assuming a linear elastic response of this medium considered as a plane surface, the elastic deformations are then in-plane. The model derived from elastic thin shell theory results in a coupled system, formed of a Laplace term and a coupling term between the two planar displacements. We rather use a simple (uncoupled, keeping only the Laplace operator) so-called membrane model governed by a Poisson equation with suitable boundary conditions, widely used as a toy model in shape identification framework Allaire (2007). This model, though being mechanically questionable, turned out to be well suited from a computational viewpoint, allowing us to perform an efficient parameter identification task, and yielding a good predictor model.

Therefore, in our simple model we will assume that at each time step $i$, the corresponding displacement field $u_i$ will satisfy

$$
\begin{cases}
-\Delta u_i = 0 \ \text{ in } \ D_i, \\
u_i = 0 \ \text{ on } M^l \cup M^r, \\
\dfrac{\partial u_i}{\partial n} = C_1 n \ \text{ on } M^t \cup M^b, \\
\dfrac{\partial u_i}{\partial n} = C_2 \kappa n + C_3 n \ \text{ on } \omega_i \setminus Z_i, \\
\dfrac{\partial u_i}{\partial n} = \begin{pmatrix} 0 \\ -C_4 \end{pmatrix} \ \text{ on } \omega_i^t \cap Z_i, \\
\dfrac{\partial u_i}{\partial n} = \begin{pmatrix} 0 \\ C_4 \end{pmatrix} \ \text{ on } \omega_i^b \cap Z_i \ .
\end{cases} \tag{2}
$$

where $n$ is the external unit normal to $\partial D_i$, $\kappa$ is the curvature of $\omega_i$ and $C_1, C_2, C_3, C_4$ are constant parameters (in this simple model) which are determined using the experimental data. We notice that allowing for a more general operator (instead of the Laplacian) and for time and space dependence of the coefficients gives us the possibility of going beyond the linear elastic, homogeneous and isotropic setting that, for simplicity, we will consider in this paper.

Once $u_i$ is obtained, we consider its restriction the leading edge $\omega_i$ and displace this boundary (using a level set method) to obtain $\omega_{i+1}$. The domain $W_{i+1}$ enclosed by $\omega_{i+1}$ is the new position of the wound. More precisely, we compute the solution $u_i$ of (2) in the domain $D_i$ by using finite element methods on a triangular mesh. We obtain a vector field $u_i$, which is used as a velocity vector in the level set method in order to move $\omega_i$.

The position of $\omega_{i+1}$ obtained also defines the new epidermal domain $D_{i+1} = M \setminus W_{i+1}$ which will be used in the following step to solve equation (2) in order to obtain $u_{i+1}$, and so on.

We remark that we are doing all our analysis in 2D while the real dynamics is 3D. In fact, we try to obtain our original data keeping as much 3D information as possible (although the embryos are still flattened by their own weight - see section 6) and avoiding to interfere with the dynamics (in preceding works the embryos were squeezed between the coverslip and a permeable membrane which, although it has the advantage of reducing the spatial shifts,

risks perturbing the movement and destroys the 3D character). However, for the moment, we project the confocal images to obtain 2D data which is simpler to treat (in particular for the contour extraction). Nevertheless, all the forces described in the model can be considered in 3D (in that case, at each point, one should naturally work on the tangent plane to the embryo at the point considered).

The model presented here is a macroscopic model that does not take into account the positions of the individual cells constituting each of the tissues considered. Thus, we can only expect to use it to obtain results at a tissue level scale and not for obtaining results at a cellular scale where the geometry of each cell and its neighbors should play an important role. However, even for more precise cellular level studies where we have to concentrate on a small patch of cells, not being able to follow in detail all the cells in our tissue, this type of macroscopic models can be useful for providing reasonable boundary or asymptotic conditions for the local problems.

This model also assumes a very simple mechanical behavior of the tissue. Our original motivation for choosing a homogeneous, isotropic and linear elastic model for the epidermis was, on the one hand, the fact that the precision of our present data did not justify more complicated assumptions and, on the other hand, the simplicity of the equations obtained (and, thanks to the linear aspect of the model, the great reduction that results for the parameter optimization procedure - see section 3). However, very recently, new techniques have been developped (see Ma et al. (2009)), which may make it possible to obtain more precise information about the forces involved. As a matter of fact, the measures concerning relaxed strain patterns and radial displacement (for hole drilling experiments in amnioserosa cells during DC) published in Ma et al. (2009) confort us in our choice of this simple model at a macroscopic scale since they indicate that:

- correlation with the individual geometry of the cell walls is significant only for distances below first neighbor distance (10 $\mu m$ in their case), and becomes considerably more isotropic beyond second neighbor separation distance;

- a linear elastic, isotropic and homogeneous sheet gives a good prediction of the observed radial displacements for distances above 10 $\mu m$.

Nevertheless, once the mechanical and 3D properties of the tissue can be determined in a more precise way, it will be interesting to include them to

improve the model.

## 3. Numerical Simulations

As said in the previous section, we assume that the dynamics of the wound is governed by equations (2) where the magnitude of the parameters $(C_j)_{1\leq j\leq 4}$ are to be identified. Let $C = (C_1, C_2, C_3, C_4)$. The aim of the numerical simulations is to identify such global coefficients $C$ by solving an optimization unconstrained problem and then compare them in a wild type and in a modified setting, in order to validate our model.

First, we obtain experimental successive boundaries of the wound by means of image processing/contour-extraction techniques. We consider at each time step $i$ the experimentally observed boundary of the wound, $\omega_i^{EXP}$, as initial boundary. For a given collection of parameters $C$, we solve the equation (2) in order to obtain a displacement $u_i$, which is used to evolve the initial boundary $\omega_i^{EXP}$ of the wound into an updated one $\omega_{i+1}^{PDE}$. Let $W_i^{EXP}$ and $W_i^{PDE}$ denote the sets enclosed by $\omega_i^{EXP}$ and $\omega_i^{PDE}$, respectively.

Since we want to identify constant (space and time independent) force coefficients $C$ which describe the whole process of closure, we consider the optimization problem consisting of minimizing the cost function $J$ given by

$$J(C) = \sum_{i=1}^{m} |W_i^{EXP} \ \Delta \ W_i^{PDE}|,$$

where $m$ is the number of time evolution steps considered in the optimization procedure and $|W_i^{EXP} \ \Delta \ W_i^{PDE}|$ denotes the area of the set of symmetric difference between $W_i^{EXP}$ and $W_i^{PDE}$, i.e. the set of elements which are in one of the sets, but not in both (exclusive disjunction in Boolean logic). The symmetric difference provides a quantification of the error to be minimized in order to obtain the correct values of the parameters $C$.

We use a global optimization approach, based on the the Genetic (`ga`) module provided by Matlab. The genetic algorithm allows to solve both constrained and unconstrained optimization problems by using biological evolution. At each step, the algorithm randomly selects individuals in a population and uses them to generate the children for the next generation. In this way the population evolves toward an optimal solution. It is a suitable method for problems where standard optimization algorithms fail to converge since the objective function is for instance discontinuous, non differentiable,

highly nonlinear, etc. In our case, the cost function $J$ is obtained by solving a PDE and then computing the area of the symmetric difference between the approximated contour and the wound. Therefore, $J$ is non-smooth and classical gradient methods are useless. Moreover, one cannot exclude the existence of multiple local minima, for which descent methods are inefficient. The genetic methods overcome these two drawbacks, but it is necessary to carefully choose the parameters (e.g. the population size, the amount of mutation, the crossover rate, etc.) to obtain accurate results. For instance, one crucial factor is the diversity of the population: if the diversity is too high or too low, the genetic algorithm might not perform well.

A well known shortcoming of the above global minimizing algorithms is that they use extensive call to cost evaluation, which in our case amounts theoretically to solve, for each time step $i$, a large number of large scale linear systems (as many as the number of generations times the number of individuals per generation).

Fortunately, we can take advantage of the linearity of (2) to solve just one partial differential equation for each significant parameter: for $j = 1, \ldots, 4$ and for each step $i = 0, \ldots, m-1$, we define $u_i^{j,1}$ to be the solution of problem (2) with $C_j = 1$ and $C_k = 0$ for $k \neq j$. Then, thanks to the linearity of our model, the solution of the full problem (2) will be given by

$$u_i = \sum_{j=1}^{4} C_j u_i^{j,1} \ . \tag{3}$$

Moreover, since in practice, as we will see in the following section, we will take $C_3 = 0$, we just have to compute $u_i^{1,1}$, $u_i^{2,1}$ and $u_i^{4,1}$. Once we have these solutions, the general solution $u_i$ will just depend linearly on the parameters $C_i$ which simplifies considerably the optimization of these parameters.

The numerical simulations are performed in Matlab code (http://www.mathworks.com/) and by using Comsol Multiphysics software (http://www.comsol.com/) to compute the numerical solution of (2) and (6) by finite elements method.

Finite element method (see for instance Quarteroni (2009)) is the most used numerical technique to approximate solutions of partial differential equations. The computation domain is subdivided into smaller regions, typically triangles or quadrilaterals in two dimensions. Over each element of the mesh, the unknown variables of the PDE are computed using polynomial expansions which depend on the nodes used to define the finite element

shape. Instead of directly discretizing the PDE, finite element method consists in multiplying the equation by a test function, chosen in a appropriate function space, integrating over the computation domain and then using the integration by parts to transfer the derivatives onto the test function. In this way, the boundary value problem is transformed into an equivalent form, called weak or variational form, which requires less regularity. The weak form is then discretized by chosing a subspace of piecewise polynomial functions (generally quadratic) which leads to solving a set of linear equations. In our case, we use a triangular mesh, quadratic polynomial functions and Umfpack direct solver for computing the solution of the linear system.

Having obtained $u_i$, we use level set methods to perform the evolution of our contour(Osher and Sethian (1988)). Level set methods (also called dynamic implicit surfaces) (Sethian (1999); Osher and Fedkiw (2003); Kimmel (2004)) are a set of popular numerical algorithms for solving a particular class of first-order hyperbolic partial differential equations, called Hamilton-Jacobi equations (HJ). Level set methods are used for tracking and simulating the motion of dynamic surfaces (in two and three dimensions) in many fields as image processing, computational fluid dynamics, seismic analysis and materials science. The front $x(t)$ at each time t is implicitly represented as the zero level set of a function $\Phi : \mathbb{R}^2 \times \mathbb{R}^+ \to \mathbb{R}$ (or $\Phi : \mathbb{R}^3 \times \mathbb{R}^+ \to \mathbb{R}$ in three dimensions), i.e. the front is given by $\Phi(x(t), t) = 0$ (see figure 3). Differentiating with respect to $t$, we obtain the Hamilton-Jacobi equation (Sethian (1999); Kimmel (2004)):

$$\partial_t \Phi(x, t) + \dot{x}(t) \cdot \nabla \Phi(x(t), t) = 0, \tag{4}$$

where $\dot{x}(t)$ is the direction of front propagation. Level set methods consist in solving (4) and then computing at each time step the propagating front as zero level set of $\Phi$. This approach requires an initial function $\Phi(x, t = 0)$ with the property that the zero level of this initial function corresponds to the initial position of the front: a possible simple choice is given by the signed distance to the front.

There are three main advantages in evolving interfaces by level set methods instead of implementing particle or Lagrangian methods: changes of topology are naturally handled and surfaces automatically merge and separate; geometric quantities, as surface normal, curvature, etc. are easy to calculate; the extension to three and even higher dimensions is conceptually straightforward.

In our case, we use level set methods to displace the leading edge $\omega_i$ by the vector field $u_i$, i.e. $\omega_i$ is the zero level set of the function $\Phi_i(x)$, solution of:

$$\partial_t \Phi_i(x,t) + u_i(x) \cdot \nabla \Phi_i(x,t) = 0. \tag{5}$$

The implicit representation of $\Phi_i$ displaces all the level sets throughout the entire computational domain, not only the zero level set. Hence, we must be able to construct an extension velocity which, starting with the velocity prescribed at the interface, builds an appropriate velocity field everywhere in the computational domain. This extension is in general not straightforward and different approaches are proposed in the literature (see Sethian (1999)). The main requirement for an extension velocity is that it smoothly approaches the prescribed interface velocity near the zero level set. In our case the velocity field has a natural extension in the domain inside the inner boundary $\omega_i$ (i.e. in the wound $W_i$): the harmonic extension obtained solving

$$\begin{cases} -\Delta u_i^{int} = 0 \ \text{ in } \ W_i, \\ u_i^{int} = u_i \ \text{ on } \omega_i. \end{cases} \tag{6}$$

In this way, we obtain an extension of the original vector field $u_i$ to the entire rectangular domain (which we will still denote by $u_i$ for simplicity). We then solve the HJ equation (5) on a regular cartesian grid by using a second order numerical finite differences scheme both in space and in time. The value of $u_i$ in the regular grid is computed by interpolating $u_i$ on triangular mesh. Due to the hyperbolic character of equation (5), upwinded approximations or artificial viscosity must be used in order to maintain stability. If the upwind propagation direction can be computed, upwind schemes yield more accurate results than artificial diffusion. At each grid point, the upwind method corresponds to approximating $\partial_x \Phi_i$ and $\partial_y \Phi_i$, the x and the y component of the gradient of $\Phi_i$, by left or right finite differences according to the direction of propagation, i.e. to the sign of the x and the y component of $u_i$. For instance for the x-component, the left $D^-\Phi(x_j)$ and right $D^+\Phi(x_j)$ first-order accurate approximation at node $(x_j, y_k)$ are

$$\begin{aligned} D^-\Phi(x_j,y_k) &= \frac{\Phi(x_j,y_k) - \Phi(x_{j-1},y_k)}{\Delta x}, \\ D^+\Phi(x_j,y_k) &= \frac{\Phi(x_{j+1},y_k) - \Phi(x_j,y_k)}{\Delta x} \end{aligned} \tag{7}$$

We perform spatial discretization by using an upwind second order Essentially Non-Oscillatory (ENO)(Osher and Shu (1991), Kimmel (2004, chap.

3)) scheme which consists of making the second order left and right correction to the first order approximation (7) and then choosing the least oscillatory of those two. The time discretization is treated by a second order total variation diminishing Runge-Kutta scheme. We use the Matlab toolbox of Ian M. Mitchell (Mitchell (2008)) (http://www.cs.ubc.ca/˜ mitchell) to implement level set methods.

## 4. Experimental results

In order to validate our model we applied it in a wild type setting and also in a modified setting (Armgal4-UAS Spastin flies) which had already been described in the literature (Jankovics and Brunner (2006)). We used ten embryos of each type and filmed them during dorsal closure. The LE positions were extracted from these films yielding the experimental contours (the $\omega_i^{EXP}$ of the previous section). The coefficients $C_j, j = 1, 2, 4$ for each embryo were then obtained using our model, as described above (see figure 6). As we mentioned before, we chose to drop the $C_3$ term since in the Dorsal curvature setting the second and third forces considered (curvature force and constant normal force) are colinear and have nearly constant relative magnitudes (since, in the sweeping phase of DC and in the wild type and the spastin setting considered here, the curvature has small variations in the central part of the LE, far from the canthi). As these two terms play nearly interchangeable roles in the settings considered, we have an approximately invariant direction of the cost function which makes it meaningless to optimize $C_2$ and $C_3$ simultaneaously. This will no longer be the case when we have more complicated geometries that appear in geneticaly modified settings that strongly affect DC (or in wound healing).

We also tested the stability of our model by computing the cost function $J$ for an adequate number of values, in order to check the continuous dependence of $J$ on the parameters and check that we do not have a great number of local minima where the minimization procedure could be trapped. For, instance, for Spastine embryo 7 we computed $J(C_1, C_2, C_4)$ with $C_1$ and $C_2$ varying from 0 to 0.3 and $C_4$ varying from 0 to 1 with constant step size 0.01. A partial representation of these values is given in figure 8. This figure give a clear indication that, at least in this case, it is unlikely for $J$ to have significant oscillations or multiple minima and that it is depends continuously on the parameters. For this embryo, the coefficients obtained by the genetic algorithm are $C = (C_1, C_2, C_4) = (0, 0.06, 0.18)$ (shown in figure 6).

## 5. Conclusion

The results obtained show very clearly that $C_4$, the zipping coefficient, is significantly downregulated in the spastine setting: figure 7 shows a considerable decrease in this coefficient (on average). This was exactly what we were looking for when we chose to use these flies based on **??**. It is thus a good point for the pertinence of our model. We notice that $C_1$, the coefficient associated with ectoderm resistance, is also downregulated. We were not looking for this effect but it is also consistent with what was described briefly in **??** and with what we observe in our own movies. In fact, we can see that the cells in the lateral epidermis of our embryos (as well as those in the engrailed bands of the en-Spastine flies in Jankovics and Brunner (2006)) are considerably less stretched in the dorso-ventral direction than those of the wild type embryos. This is an indication that the tension on these cells should be lower than in the wild-type and it is thus normal to have a lower value for $C_1$ in the Spastine embryos.

Another point that is a good indication concerning our approach is the fact that inside each group, the coefficients measured for the different members are quite consistent - i.e. the dispersion of the data is relatively low (except for the last fly in the Spastine group which seems to zip nearly like a wild-type). Moreover, the data we show in the previous section is just for the 10 wild type flies which are the natural control for the spastine flies used. However, we also calculated these coefficients for several different wild-type fly lines we have filmed for other purposes, and the values obtained were close to the ones shown here (data not shown).

To illustrate the precision that we can attain with the present model, we show in figures 9 and 10 the simulated contours using our model in a Spastin embryo (which is less precise than in the wild type case) using the optimal constant force parameters we obtained.

## 6. Appendix: Material and Methods

## 7. Movie Captions

Allaire, G., 2007. Conception optimale de structures. Vol. 58 of Mathématiques & Applications (Berlin) [Mathematics & Applications]. Springer-Verlag, Berlin, with the collaboration of Marc Schoenauer (INRIA) in the writing of Chapter 8.

Almeida, L., Bagnerini, P., Habbal, A., Noselli, S., Serman, F., 2009. Tissue repair modeling. Singularities in Nonlinear Evolution Phenomena and Applications, 27–46.

Hutson, M. S., Tokutake, Y., Chang, M.-S., Bloor, J. W., Venakides, S., Kiehart, D. P., Edwards, G. S., Apr 2003. Forces for morphogenesis investigated with laser microsurgery and quantitative modeling. Science 300 (5616), 145–149.
URL http://dx.doi.org/10.1126/science.1079552

Jacinto, A., Wood, W., Balayo, T., Turmaine, M., Martinez-Arias, A., Martin, P., Nov 2000. Dynamic actin-based epithelial adhesion and cell matching during drosophila dorsal closure. Curr Biol 10 (22), 1420–1426.

Jankovics, F., Brunner, D., Sep 2006. Transiently reorganized microtubules are essential for zippering during dorsal closure in drosophila melanogaster. Dev Cell 11 (3), 375–385.
URL http://dx.doi.org/10.1016/j.devcel.2006.07.014

Kiehart, D. P., Galbraith, C. G., Edwards, K. A., Rickoll, W. L., Montague, R. A., Apr 2000. Multiple forces contribute to cell sheet morphogenesis for dorsal closure in drosophila. J Cell Biol 149 (2), 471–490.

Kimmel, R., 2004. Numerical geometry of images. Springer-Verlag, New York, theory, algorithms, and applications.

Ma, X., Lynch, H. E., Scully, P. C., Hutson, M. S., 2009. Probing embryonic tissue mechanics with laser hole drilling. Phys Biol 6 (3), 036004.
URL http://dx.doi.org/10.1088/1478-3975/6/3/036004

Millard, T. H., Martin, P., Feb 2008. Dynamic analysis of filopodial interactions during the zippering phase of drosophila dorsal closure. Development 135 (4), 621–626.
URL http://dx.doi.org/10.1242/dev.014001

Mitchell, I. M., 2008. The flexible, extensible and efficient toolbox of level set methods. J. Sci. Comput. 35 (2-3), 300–329.

Murray, J. D., 2003. On the mechanochemical theory of biological pattern formation with application to vasculogenesis. Comptes Rendus Biologies

326 (2), 239 – 252.
URL http://www.sciencedirect.com/science/article/B6X1F-4893WR0-7/2/c8300e5b2f07

Olsen, L., Maini, P. K., Sherratt, J. A., 1998. Spatially varying equilibria of mechanical models: application to dermal wound contraction. Math. Biosci. 147 (1), 113–129.
URL http://dx.doi.org/10.1016/S0025-5564(97)00075-8

Olsen, L., Sherratt, J. A., Maini, P. K., 1995. A mechanochemical model for adult dermal wound contraction and the permanence of the contracted tissue displacement profile. Journal of Theoretical Biology 177 (2), 113 – 128.
URL http://www.sciencedirect.com/science/article/B6WMD-45R8FPF-F/2/8bd33dd039cb

Osher, S., Fedkiw, R., 2003. Level set methods and dynamic implicit surfaces. Vol. 153 of Applied Mathematical Sciences. Springer-Verlag, New York.

Osher, S., Sethian, J. A., 1988. Fronts propagating with curvature-dependent speed: Algorithms based on hamilton-jacobi formulations. J. Comput. Phys. 79 (1), 12–49.

Osher, S., Shu, C.-W., 1991. High-order essentially nonoscillatory schemes for hamilton-jacobi equations. SIAM J. Numer. Anal. 28 (4), 907–922.

Peralta, X. G., Toyama, Y., Hutson, M. S., Montague, R., Venakides, S., Kiehart, D. P., Edwards, G. S., Apr 2007. Upregulation of forces and morphogenic asymmetries in dorsal closure during drosophila development. Biophys J 92 (7), 2583–2596.
URL http://dx.doi.org/10.1529/biophysj.106.094110

Quarteroni, A., 2009. Numerical models for differential problems. Vol. 2 of MS&A. Modeling, Simulation and Applications. Springer-Verlag Italia, Milan.

Sethian, J. A., 1999. Level set methods and fast marching methods, 2nd Edition. Vol. 3 of Cambridge Monographs on Applied and Computational Mathematics. Cambridge University Press, Cambridge.

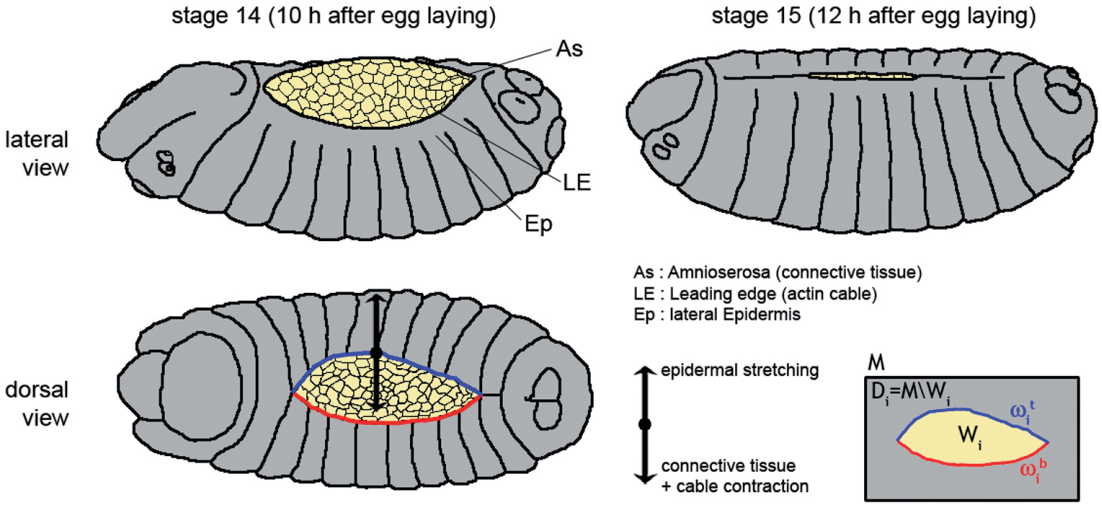


Figure 1: Scheme of tissues and forces implicated in dorsal closure in Drosophila embryos. The first row shows a dorso-lateral drawing of the drosophila embryo at stages 14 and 15. The second row shows a dorsal view of a stage 14 embryo and a representation of some of the forces involved in the closure. Lines indicate the two tissues involved (the connective tissue of the amnioserosa consisting of thin and large polygonal epithelial cells in yellow, the epidermis consisting of columnar epithelial cells in gray) and in-between the Leading Edge (LE). In the last diagram we distinguish the LE's top margin $\omega_i^t$ (in blue) and bottom one $\omega_i^b$ (in red).

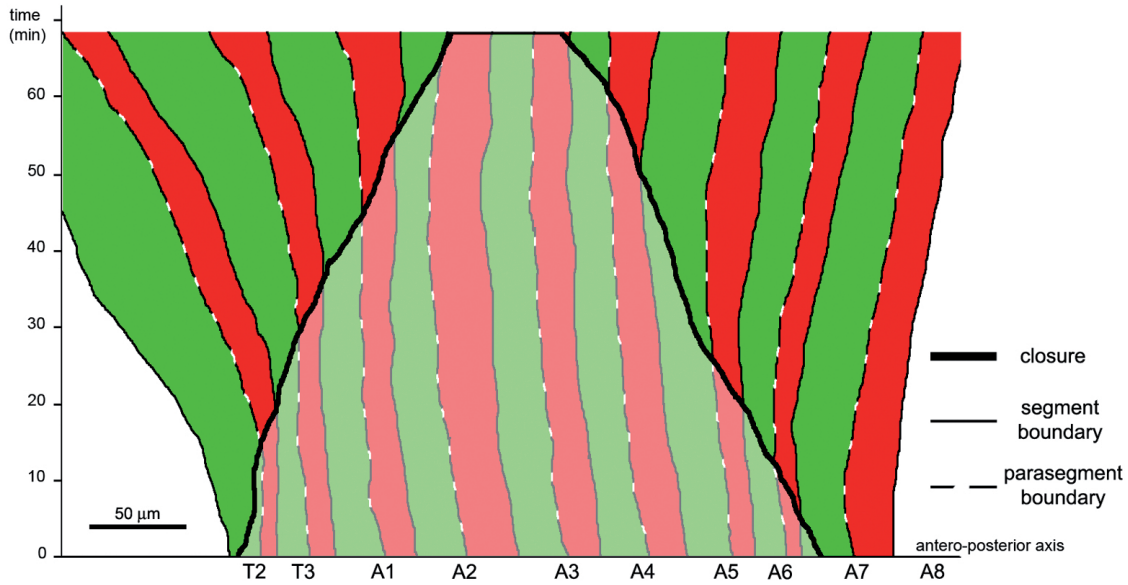


Figure 2: Antero-posterior stretching of segmental boundaries during dorsal closure. The central curve (bold line) shows the closure of each parasegmental and segmental boundaries during time, from a total opening (the exposed amnioserosa extends from segment T2 to segment A7 at time 0) nearly up to the end of closure (the exposed amnioserosa covers only parts of segments A2 and A3 at time 70'). The solid and dashed lines indicate the positions of segmental and parasegmental boundaries at each time, respectively. These curves were obtained by tracking the half-segment boundaries during the dorsal closure of the embryo shown in movie `track.mov`.

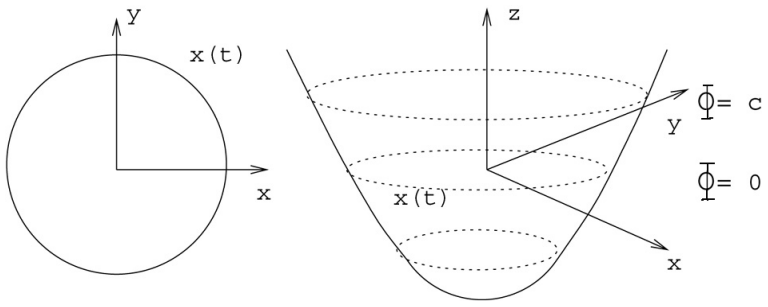


Figure 3: At each time $t$ the propagating front $x(t)$ is the zero level set of a function $\Phi(x(t), t)$ solution of a Hamilton-Jacobi equation.

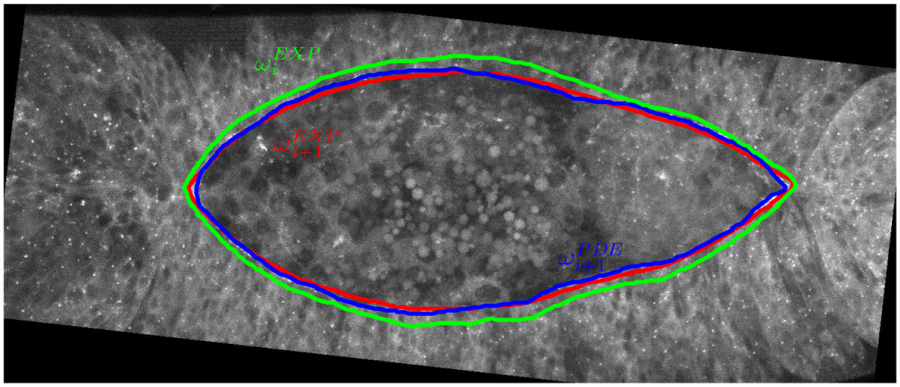

Figure 4: Example of experimentally observed boundaries of the wound at time step $i$ ($\omega_i^{EXP}$ in green) and $i+1$ ($\omega_{i+1}^{EXP}$ in blue), and of the simulated contour $\omega_{i+1}^{PDE}$ (in red)

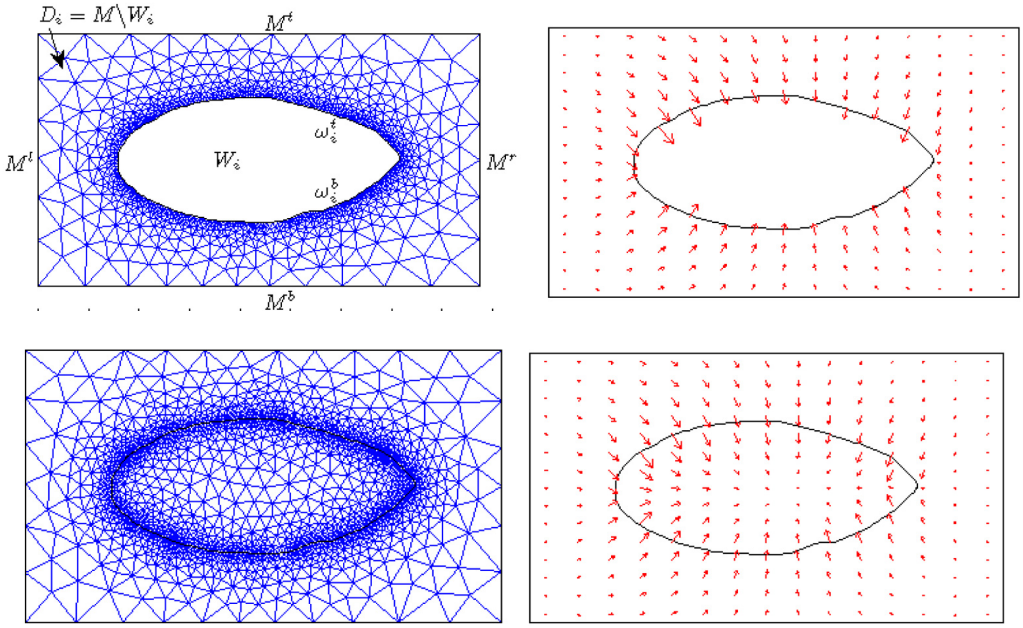


Figure 5: Example of a computed solution $u_i$ alone (top right) and together with its associated extension $u_i^{int}$ (bottom right) and the corresponding computational meshes (left).

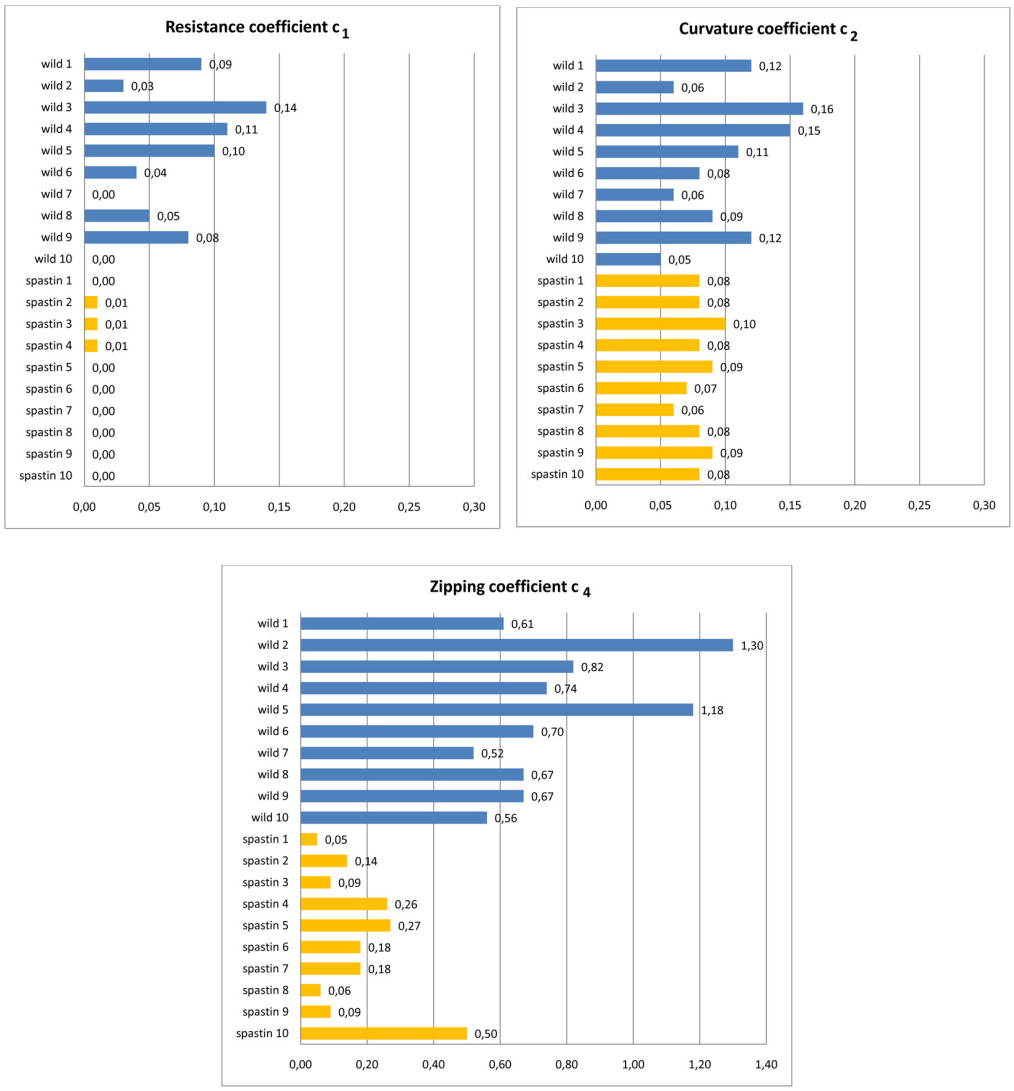


Figure 6: The optimized coefficients $C_1$, $C_2$, $C_4$ of ten wild type and ten mutant (Armgal4-UAS Spastin) embryos.

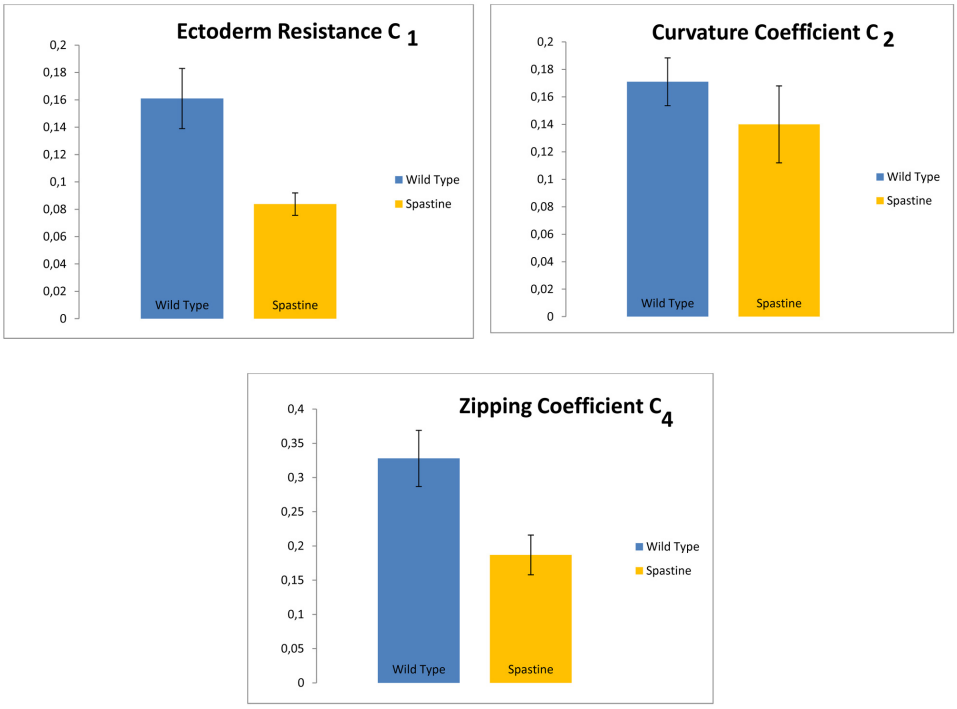


Figure 7: Average of the optimized coefficients $C_1$, $C_2$, $C_4$ of ten wild type and ten mutant (Armgal4-UAS Spastin) embryos.

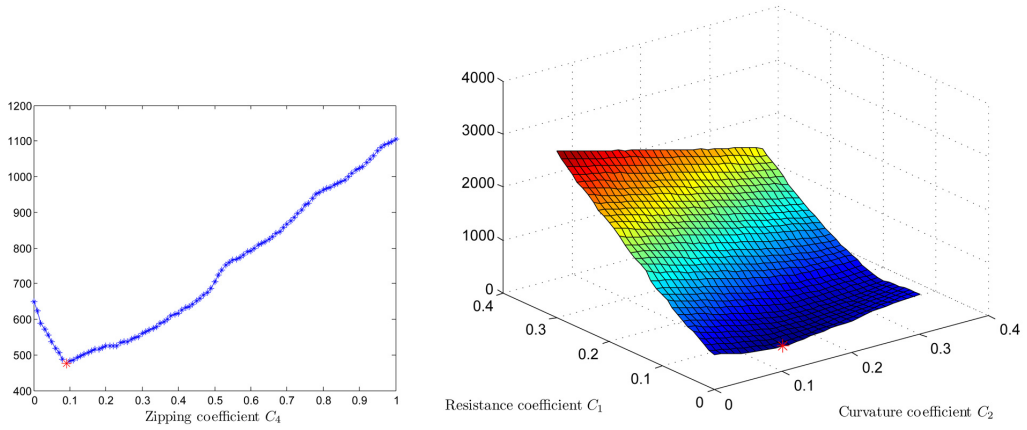


Figure 8: On the left, for each fixed value $C_4$, we show the minimum of the two dimensional function $J(\cdot, \cdot, C_4)$ in the interval $[0, 0.3] \times [0, 0.3]$, computed with constant step size 0.01. On the right, we show the cost surface $J(\cdot, \cdot, 0.18)$, i.e. corresponding to the minimum $C_4 = 0.18$ (the red point $(C_1, C_2) = (0, 0.06)$ minimizes this section of the cost function).

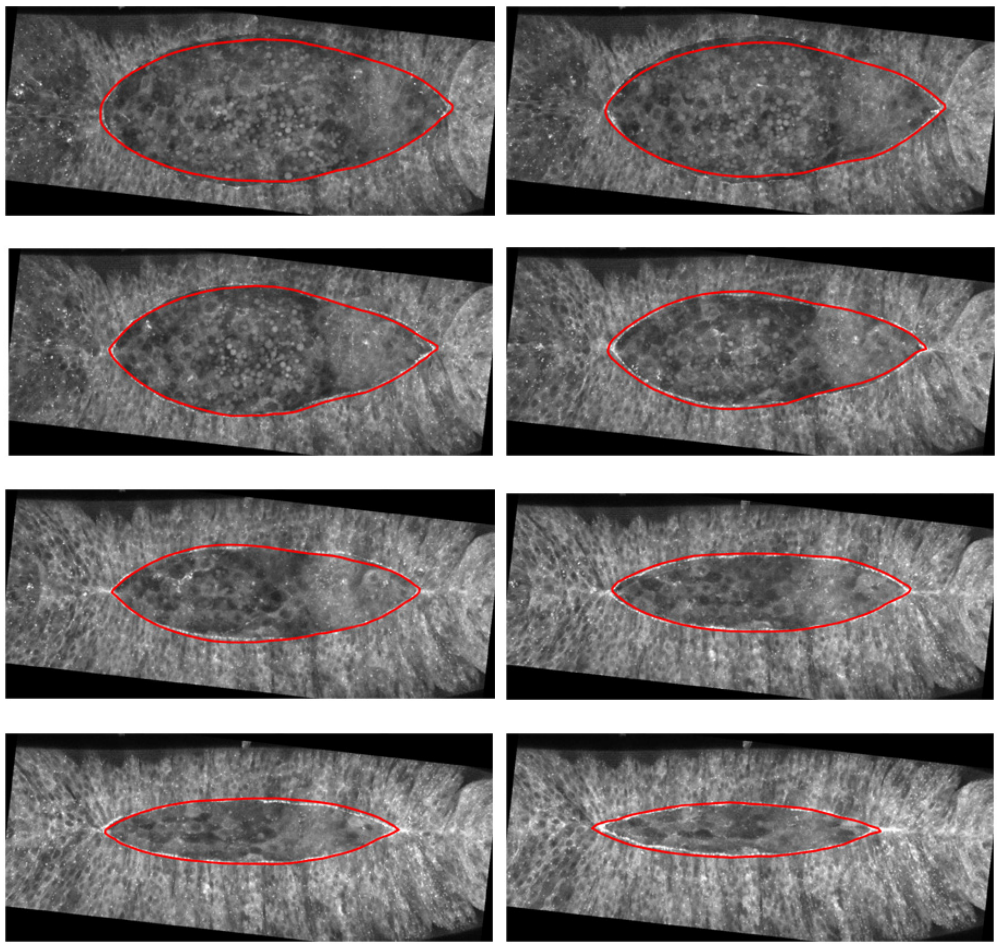

Figure 9: Dorsal Closure images at successive times with corresponding simulated contours (in red) for a Spastin embryo: first eigth images.

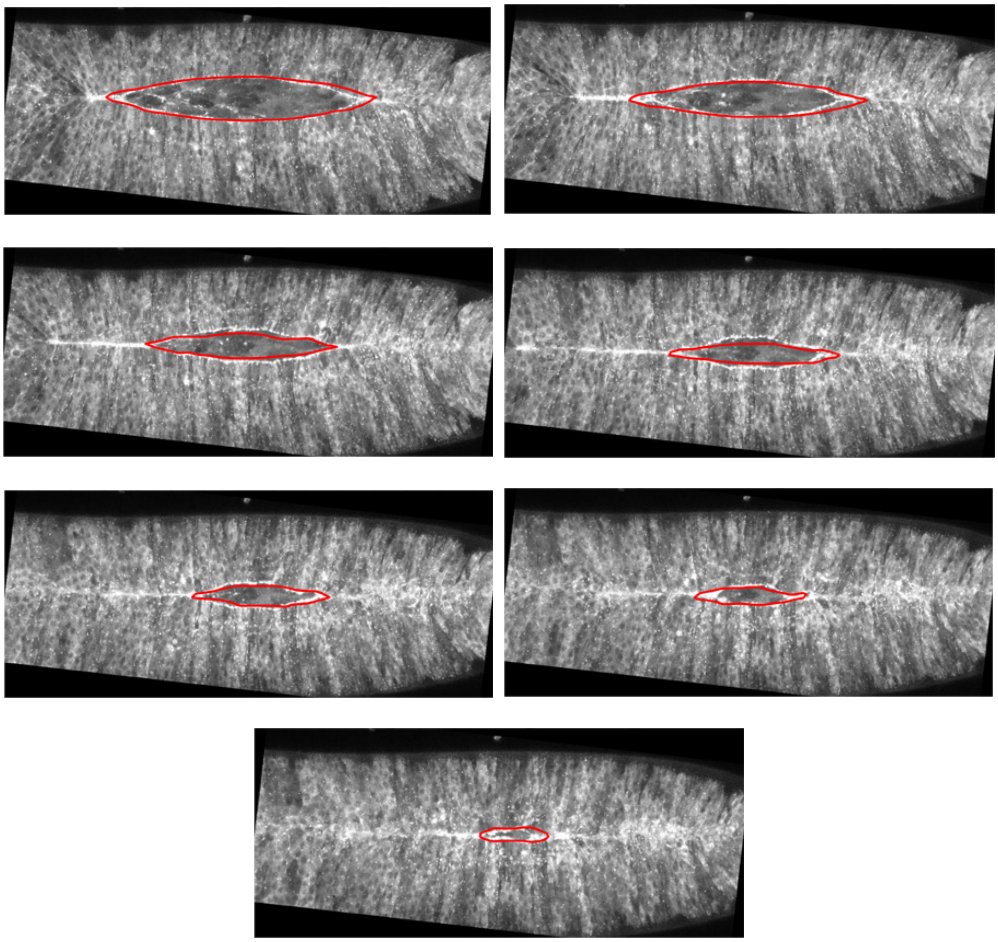

Figure 10: Dorsal Closure images at successive times with corresponding simulated contours (in red) for a Spastin embryo: final seven images.